Research Report

Analysis of Fast Dynamic Processes in Living Cells: High-Resolution and High-Speed Dual-Color Imaging Combined with Automated Image Analysis

BioTechniques 28:722-730 (April 2000)

A. Rustom, D. Gerlich, R. Rudolf, C. Heinemann[1], R. Eils and H.-H. Gerdes
University of Heidelberg, Heidelberg, Germany, and [1]T.I.L.L. Photonics GmbH, Martinsried, Germany

ABSTRACT

The generation of spectral mutants of the green fluorescent protein (GFP) set the stage for multiple-color imaging in living cells. However, the use of this technique has been limited by a spectral overlap of the available GFP mutants and/or by insufficient resolution in both time and space. Using a new setup for dual-color imaging, we demonstrate here the visualization of small, fast moving vesicular structures with a high time resolution. Two GFP-fusion proteins were generated: human chromogranin B, a secretory granule matrix protein, and phogrin, a secretory granule membrane protein. They were tagged with enhanced yellow fluorescent protein (EYFP) and enhanced cyan fluorescent protein (ECFP), respectively. Both fusion proteins were cotransfected in Vero cells, a cell line from green monkey kidney. EYFP and ECFP were excited sequentially at high time rates using a monochromator. Charged coupled device (CCD)-based image acquisition resulted in 5–8 dual-color images per second, with a resolution sufficient to detect transport vesicles in mammalian cells. Under these conditions, a fully automated time-resolved analysis of the movement of color-coded objects was achieved. The development of specialized software permitted the analysis of the extent of colocalization between the two differentially labeled sets of cellular structures over time. This technical advance will provide an important tool to study the dynamic interactions of subcellular structures in living cells.

INTRODUCTION

Single-color imaging of cellular dynamics with the green fluorescent protein (GFP) has become a standard approach in many cell biological studies (2,4,11,14). This technique has led to exciting new insights into diverse cellular processes such as distinct steps of membrane traffic in the secretory pathway. These observations have generated questions concerning the dynamic interactions between the different types of components involved and have necessitated the development of multicolor imaging systems that permit the simultaneous visualization of at least two proteins and a comparison of their distribution in live cells. Several promising approaches in this direction have been reported during the last two years.

Using confocal time lapse imaging, Zimmermann and Siegert (18) were able to simultaneously detect two spectral mutants of GFP, W2 (6) and S65T (5). However, this approach was impeded by a spectral overlap of the two GFP mutants, which resulted in insufficient separation of their fluorescence signals. Moreover, the confocal setup provided a low time resolution that was not suitable for the analysis of fast cellular dynamics. In a later study, the use of a new pair of spectral GFP variants, the blue-shifted variant W7 (6) and red-shifted variant 10C (3), led to a clean separation of both fluorescence signals either by a confocal microscope or a wide-field fluorescence microscope equipped with a filter wheel (3). These dual-color imaging systems were shown to be well suited for time-lapse recordings (3), but, due to the hardware-specific limitations of their image acquisition rates, they were insufficient for the analysis of fast dynamics such as vesicular transport.

Based on the well-established blue- and yellow-shifted GFP variants, we describe here a powerful multicolor imaging system (Figure 1) capable of imaging small subcellular structures with a high time resolution. This is exemplified by the visualization of small and fast-moving vesicular structures. Furthermore, we extended a recently developed software package (15) to achieve a fully automated and unbiased analysis of dual-color imaging data. The objects of both channels were automatically detected and tracked, and their dynamic colocalization in time and space was determined.

MATERIALS AND METHODS

Cloning of GFP Fusion Proteins

hCgB-EYFP: A DNA fragment encoding hCgB, originally obtained from the expression vector pCDM8/hCgB-EGFP (10) by restriction with *Hin*dIII/*Kpn*I, was ligated into the *Hin*dIII/*Kpn*I-digested pEYFP-N1 vector (Clontech Laboratories, Palo Alto, CA, USA).

Phogrin-ECFP: A cDNA fragment encoding phogrin was generated by

PCR using a pcDNA3-phogrin construct (17) as a template. For this PCR, the oligonucleotides *Bgl*II-phogrin, (5′-CGACGAAGATCTCATGGGGCTACCGCTCCCGCTTTTG-3′) and phogrin-*Eco*RI, (5′-CGTCGGAATTCTCTGGGGAAGGGCCTTCAGGATGGC-3′) were used as forward and reverse primers, respectively. The underlined sequences indicate *Bgl*II and *Eco*RI restriction sites introduced by the PCR. The PCR fragment was digested with *Bgl*II/*Eco*RI and subcloned into the pECFP-N1 vector (Clontech Laboratories) opened with *Bgl*II/*Eco*RI.

Cell Culture and Transfection

Vero cells (ATCC CCL 81) were grown at 37°C in EMEM supplemented with 10% fetal calf serum and 2 mM glutamine at 5% CO_2. Cells were transiently co-transfected with hCgB-EYFP and phogrin-ECFP by electroporation using a Gene Pulser™ (Bio-Rad Laboratories, Hercules, CA, USA). Electroporation was performed with 25 µg DNA of each plasmid in a total volume of 0.8 mL cell suspension (harvested from one confluent 15 cm culture dish) at 960 µF and 300 V. The transfected cells were diluted in 30 mL culture medium and plated onto LabTek® coated 4-chambered cover glasses (Nalge Nunc International, Wiesbaden, Germany). After 24 h of incubation (5% CO_2 at 37°C) the cells were treated with 2 mM sodium butyrate for 21 h. The culture medium was exchanged by block medium (culture medium supplemented with 10 mM HEPES-KOH, pH 7.4), and the cells were incubated at 20°C for 2 h. Thereafter, the block medium was replaced by prewarmed culture medium, and the cells were transferred to the microscope stage.

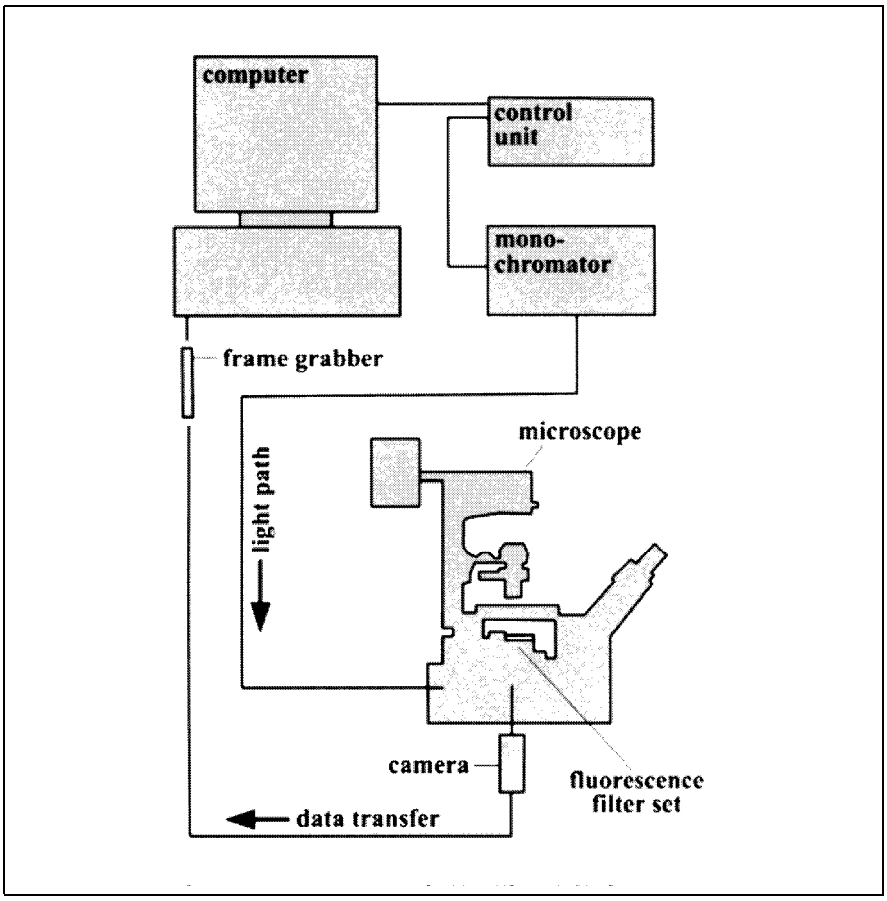

Figure 1. Diagram of the dual-color imaging setup. Excitation light produced by a monochromator is guided to an inverted microscope equipped with appropriate fluorescence filter sets. Emitted fluorescence light is captured at a side port by a Till IMAGO CCD camera connected to a 12-bit frame grabber. TILLvisION software synchronizes via a control unit both the monochromator and the camera.

Fluorescence Microscopy and Image Acquisition

High-speed, dual-color fluorescence measurements were performed with an imaging system (Figure 1, T.I.L.L. Photonics GmbH, Martinsried, Germany) attached to the inverted microscope IX-70 (Olympus Optical Europa GmbH, Hamburg, Germany). The microscope was equipped with a 100× Plan Apo™ 100×/1.40 NA oil objective (Olympus Optical) heated to 37°C by a custom-made jacket. A monochromator-based light source Polychrome II with a built-in 75 W Xenon arc lamp was used for fluorescence excitation. Any excitation wavelength in the range between 320 and 680 nm could be selected in less than 3 ms by the control of a galvanometric scanner. The bandwidth of the excitation light in this system was 15 nm (half maximum full width). To achieve maximal excitation intensity and homogeneity, the excitation light was focused with a special epifluorescence condenser (T.I.L.L. Photonics GmbH) to a spot of 125 µm that covers the camera's field of view. For dual-color imaging of EYFP and ECFP, a dichroic mirror (reflection maxima at 430 and 510 nm) and a dual-band emission filter (470/30 nm and 555/40 nm) referred to as CY+10 was used (Chroma Technology, Brattleboro, VT, USA). Single-color EYFP imaging was performed with a short pass excitation filter B51 (50% transmission at 505 nm, Balzers Thin Films, Liechtenstein), a dichroic mirror Q515LP and an emission filter HQ535/30M (Chroma Technology). We refer to this filter set as SP-EYFP. The fluorescence light was detected at the side port of the IX-70 with the IMAGO (T.I.L.L. Photonics GmbH), a Peltier cooled slow-scan interline transfer camera equipped with a Super VGA chip (1280 × 1024 pixels, pixel size 6.7 × 6.7 µm, readout noise of 7.7 electrons, A/D conversion factor of 5 electrons per pixel count) or a VGA chip (640 × 480 pixels, pixel size of 9.9 × 9.9 µm, readout noise of 13.5 electrons, A/D conversion factor of 7.5 electrons per pixel count).

Image acquisition was controlled by TILLvisION software. The 12-bit data were sampled from the charge-coupled device (CCD) chip at a rate of 12.5

MHz. The resulting transfer time for a full frame was 125 and 32 ms for the Super VGA and VGA chip, respectively. Sequences can be acquired in a continuous or bursting mode. In the continuous acquisition mode, a new image is captured after the readout of the previous one, while in the bursting mode the exposure of a new image overlaps with the readout of the previous one. The bursting mode makes use of two memory banks, each with a storage capacity of 8 MB. Data acquisition in the burst mode exceeding 8 MB leads to a discontinuity in image acquisition. For dual-color imaging, corresponding frame pairs (cycles) were recorded in the burst mode, whereas, from cycle to cycle, the continuous mode was used. This way of image acquisition not only minimized the time shift between corresponding channel recordings but also led to equidistant cycle times. The exact timing of the image acquisition and the highly synchronized exposure were controlled by an external processor board (Imaging System Controller).

Automated Image Analysis and Quantitative Measurements

For single-color imaging, fully automated object detection and tracking, as well as the visualization of trajectories using time as a third spatial dimension, was performed according to Tvaruskó et al. (15). The resulting trajectories of fluorescent structures comprise all the computing parameter information including velocity, acceleration or diffusion coefficients (15). For dual-color imaging, object detection and dynamic tracking of two-color datasets was carried out sequentially on each channel as described for single-color imaging. For continuous time-space visualization, every channel was assigned to a corresponding color (red for the EYFP channel and green for the ECFP channel), and the time shift resulting from sequential image acquisition was considered for time-axis values. Automated analysis of the colocalization between vesicular structures from different channels was determined from the continuous trajectory reconstruction by newly developed software. The distance to the gravity center of the other channel's nearest trajectories was determined. Using a distance threshold in the order of the apparent vesicle diameter (in our case, six pixels of an image acquired with a Super VGA chip), colocalization in space and time was calculated. The number of vesicles with a nearest neighbor in the other channel located nearer than the distance threshold was related to the total number of vesicles at a specific interpolated time section. The average of this value was determined over all interpolated time sections. The visualization of colocalization in time-space was displayed by blending to a third color (yellow) that was dependent on the distance of the trajectories.

RESULTS AND DISCUSSION

Dual-Color Imaging and Automated Particle Tracking

In contrast to dual-color, time-lapse imaging of slow cellular processes (3,18), real-time imaging of fast dynamic processes requires substantially higher image acquisition rates. In addition, real-time imaging of small subcellular structures down to the size of transport vesicles requires a high spatial resolution. This leads to large data sets and slower image acquisition. The challenge was to establish an imaging system that achieved high resolution in both time and space.

To develop high-speed multicolor imaging of small, fast-moving objects in living cells, we have chosen vesicular transport steps in the secretory pathway. To label vesicular structures, two fusion proteins were generated. First, human chromogranin B (hCgB), a matrix protein of neuroendocrine secretory granules (8), was fused at its C-terminus with EYFP. A similar fusion protein, hCgB-tagged at its C-terminus with the GFP(S65T) mutant, was shown to label constitutive secretory vesicles when expressed in HeLa (9) and Vero Cells (16). Second, phogrin, a type I transmembrane protein of secretory granules in insulinoma cells (17), was fused C-terminally with ECFP. A similar fusion protein, phogrin-tagged with enhanced GFP (EGFP), was used to label secretory granules of insulin-secreting cells (13). Together with the observation that a homologue of phogrin, ICA512, is transported to the plasmamembrane (PM) when ectopically expressed in fibroblast-like CHO cells (7), it can be assumed that in Vero cells, phogrin-ECFP exits the trans Golgi network (TGN) in constitutive secretory vesicles.

After co-transfection with hCgB-EYFP and phogrin-ECFP, the expression of the CMV promoter-driven fusion proteins in Vero cells was induced by sodium butyrate treatment. To accumulate the GFP fusion proteins in the TGN, the donor compartment for secretory vesicles, we applied a 20°C secretion block for 2 h (9,12). The secretion block was reversed by transferring the cells to the microscope stage heated to 37°C. EYFP and ECFP were sequentially excited by a monochromator at 505 and 433 nm. Forty digital images were captured with an exposure time of 50 ms for both emission channels, resulting in a total illumination time of 4 s. Sequential excitation in combination with optimized filter sets thereby prevented spectral crosstalk between the single-channel recordings.

At the same time, the temporal shift of corresponding images caused by the sequential excitation was minimized by the use of a monochromator that switched between the two wavelengths within less than 3 ms and by image acquisition in a burst mode. Using a Super VGA chip (6.7×6.7 µm pixel size) that provided sufficient spatial resolution to resolve vesicular structures, we achieved acquisition rates of five frame pairs per second. The first frame pair of this sequence is shown in Figure 2, A (hCgB-EYFP) and B (phogrin-ECFP). In both cases, fluorescent punctate structures throughout the cytoplasm are visible, although the signals for phogrin-ECFP are less distinct and sometimes tubular. These structures are more prominent in the perinuclear region. Additionally, for phogrin, a weak staining of the PM was detectable when the cell surface was in focus (data not shown). The overlay of frame A and B in Figure 2 reveals the colocalization of distinct hCgB-EYFP- and phogrin-ECFP-positive structures predominantly in the perinuclear region (Figure 2C). Under the same experimental settings if images were captured with a VGA chip (9.9×9.9 µm pixel size) still sufficient to detect distinct vesicular

structures (for comparison, see Figure 4), eight frame pairs per second could be acquired due to the shorter read-out time of the chip (data not shown).

With the setup used here, a further increase in image acquisition rates would be possible by reducing the exposure time and/or the image size. Likewise, the use of the burst mode and/or binning during image acquisition would lead to a gain in time resolution. A gain of temporal resolution by these means may be necessary for special applications such as calcium imaging. However, in our application, the gain in time resolution using the above procedures did not justify the loss of important image information. We could demonstrate that under our experimental conditions, a further reduction of the exposure time down to 10 ms, which resulted in an acquisition rate of 15 frame pairs per second, led to a substantial decrease of the signal-to-noise ratio (not shown). Under these conditions, an accurate automated analysis of vesicle dynamics was difficult to obtain. Binning, while increasing the signal-to-noise ratio, would also have hampered the automated analysis by the loss of spatial resolution. The use of a small area of interest (AOI) is particularly critical for the analysis of cellular transport over long distances, which requires imaging

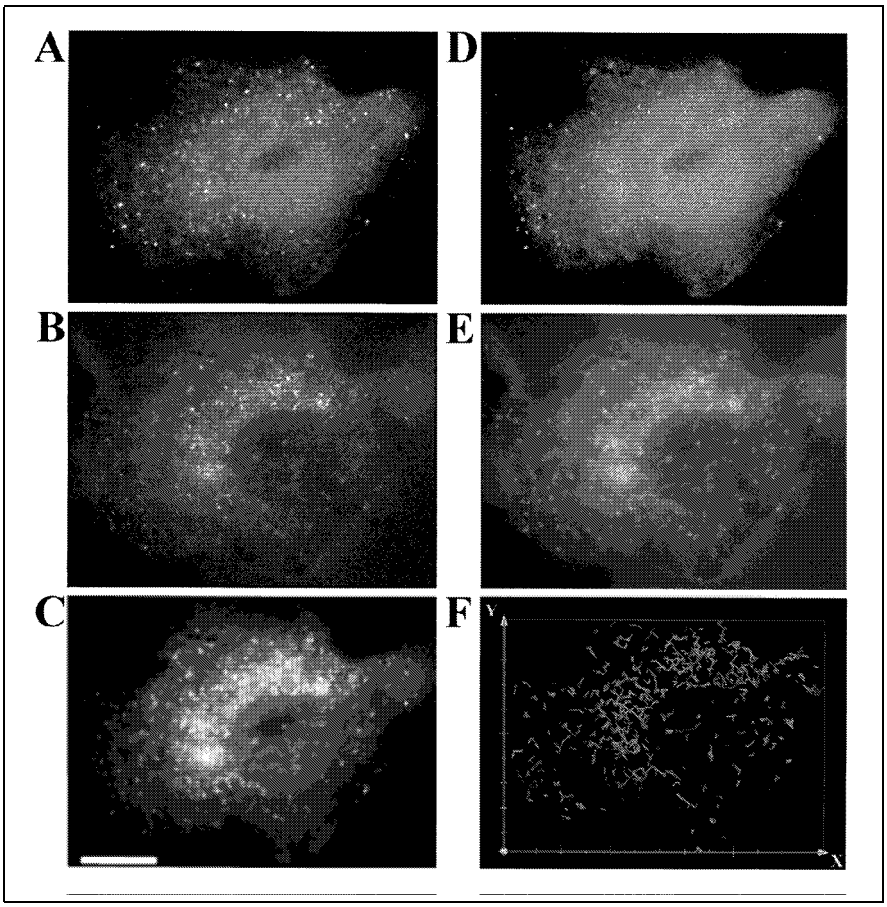

Figure 2. Dual-color imaging and automated image analysis. Vero cells were co-transfected with hCgB-EYFP and phogrin-ECFP. Fluorescence microscopy was performed 30 min after release of a 20°C secretion block by using the CY+10 filter set (see Materials and Methods). EYFP and ECFP were sequentially excited using a 50 ms exposure time for each channel. For image acquisition (Super VGA chip-equipped camera), an AOI of 725 × 541 pixels was used. Forty consecutive frame pairs with a cycle time of 197 ms were imaged. Single-channel recordings of one frame pair are shown for hCgB-EYFP (A) and phogrin-ECFP (B). The overlay of both images is shown in panel C. Note that yellow indicates colocalization. The original images were smoothed by anisotropic diffusion and subjected to edge-orientated segmentation. The identified objects are indicated by red circles for hCgB-EYFP (D) and by green circles for phogrin-ECFP (E). The movements of these objects were automatically tracked and displayed as two-dimensional (X,Y) trajectories in the respective color code (F). Scale bar = 10 μm. A dual-color movie of the complete sequence that corresponds to panel C can be viewed at http://www.nbio.uni-heidelberg.de/Gerdes.html.

of a large area of the cell. Finally, the burst mode for dual-color imaging has the advantage of providing a higher time resolution. However, in our example, the large data sets of image sequences that exceeded by far the 8 MB storage capacity of one frame grabber memory bank would have led to discontinuity in time resolution (i.e., short image sequences with equidistant time resolution interrupted by time gaps). We therefore favored the acquisition of images in the continuous mode.

For the automated analysis of dynamic fluorescent structures, we used an image analysis software package (15). After automated object detection, the identified vesicular structures for hCgB-EYFP (Figure 2D, red circles) and phogrin-ECFP (Figure 2E, green circles) show high correspondence with the fluorescence signals of the original images of Figure 2, A and B, respectively. To test the accuracy and reproducibility of the segmentation step, a quantitative analysis of automatically detected objects matching with manually identified objects was performed for the first two and the last two frame pairs of the sequence shown in Figure 2. This revealed a correspondence of 85% ± 4.2% for hCgB-positive structures (n = 541) and 90% ± 1.6% for phogrin-positive structures (n = 698). The tracks of all recognized fluorescent structures were obtained by a particle tracking module and are displayed in red (hCgB-EYFP) and green (phogrin-ECFP) in Figure 2F.

Automated Evaluation of Colocalization in Space and Time

With sequential image acquisition, the objects of both channels are shifted proportionally to their speed (Figure 3D, II). For this reason, the overlay of corresponding channel recordings (Figure 2C) is not an accurate method to measure the extent of colocalization between moving objects. To overcome this problem, time-space information of particles was used to interpolate a continuous time-space reconstruction. In the three-dimensional view of the interpolated reconstruction (Figure 3A), the extent of colocalization between red and green trajectories is encoded by blending to yellow (schematically shown in Figure 3B). Dynamic colocalization can be observed in a magnification of the interpolated time-space reconstruction (Figure 3C). A few colocalizing trajectories show little dynamics and evolve nearly parallel to the time axis. One yellow trajectory indicates two objects moving together with an average speed of 1 µm/s over the observed time period of approximately 1.6 s (arrowhead). The time shift of these objects caused by the sequential image acquisition was 72 ms as schematically illustrated in Figure 3D, II, and is much shorter than the cycling time of 197 ms as shown in Figure 3D, I. The amount of colocalization for all objects was calculated from the interpolated time-space reconstruction. For the image sequence consisting of 40 frame pairs (Figure 2), a colocalization of 27.9% was determined by averaging over all time frames. Given the fact that after its transport to the PM phogrin is transiently exposed at the cell surface and subsequently transported along the endocytic pathway, this extent of colocalization may therefore reflect only phogrin in constitutive transport vesicles.

Automated Analysis of Secretory Vesicle Movement at Velocities in the Range of Fast Axonal Transport

Besides being limited by the speed of the hardware (e.g., the readout time of the CCD camera), the image acquisition rate depends on the signal-to-noise

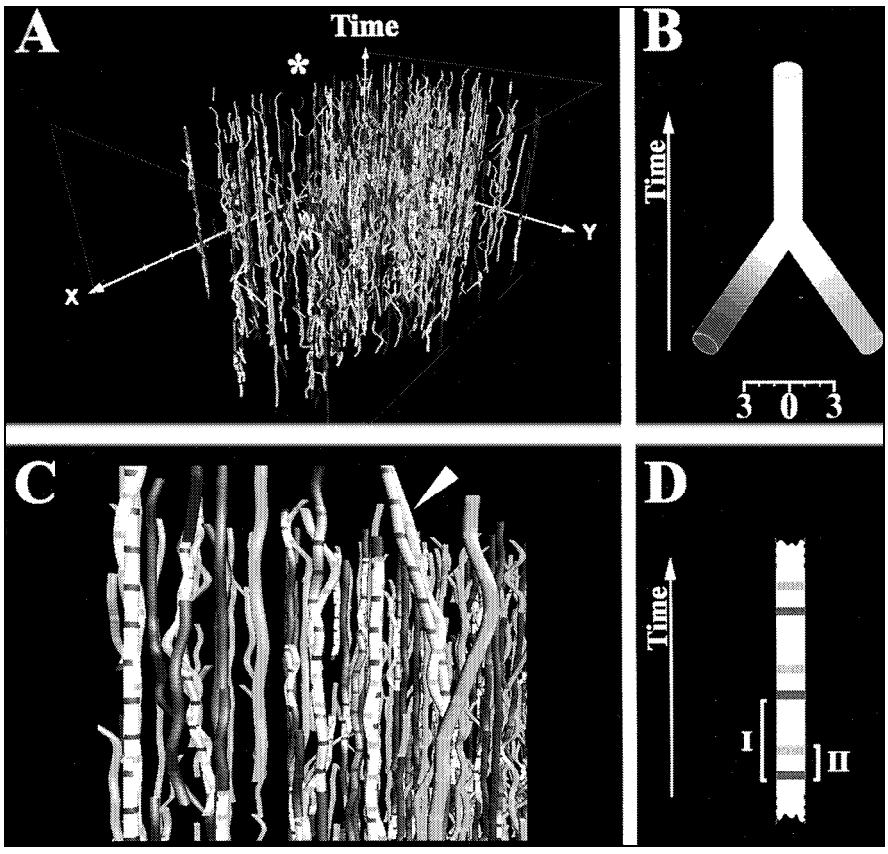

Figure 3. Visualization of trajectories and their colocalization in time and space. Trajectories of hCgB-EYFP (red) and phogrin-ECFP (green) corresponding to Figure 2 are displayed in three dimensions with time evolving along the Z-axis (A). The extent of colocalization between red and green trajectories is encoded by blending to yellow. Blending starts below a threshold of six pixels as schematically depicted (B, scale bar is in pixels). Note that complete colocalization is displayed as pure yellow. A magnification of a volume section (A, asterisk) is shown in panel C. The channel color code is highlighted by red and green rings. The segmentation of trajectories by red and green rings indicates the time steps for single-frame acquisition. Arrowhead indicates two objects moving together at an average of 1 µm/s over 8 frames. Schematic view (D) of the image acquisition mode for dual-color recordings. The time between two red rings (197 ms) represents one image acquisition cycle (I). The time shift of corresponding red and green channel recordings is 72 ms (II).

ratio sufficient for object detection. The VGA chip with a faster readout was chosen to "drain" the hardware. To further increase the image acquisition rate, single-channel recordings were performed, and the AOI was reduced to 323 × 249 pixels sufficient for capturing a small Vero cell. Under these conditions, cells that were co-transfected with hCgB-EYFP and phogrin-ECFP were imaged in the EYFP channel by using the continuous acquisition mode. Two hundred consecutive frames were recorded with 20 ms exposure time, resulting in a cycling time of 42 ms and a total illumination time of 4 s. Figure 4A shows the last image of this sequence. Despite the high time resolution, the secretory vesicles are visible as clear bright spots, which suggests that the signal-to-noise ratio would have allowed even higher frame rates. In addition, no obvious reduction of the fluorescence signals from bleaching was observed. One reason is that the tight synchronization of the excitation light source with the image acquisition system minimizes the total illumination time drastically and thereby also reduces phototoxic effects. Second, it is a well-documented fact that the GFP spectral variants of GFP used here are of reasonable photostability when used for confocal time-lapse imaging (3).

To obtain an unbiased analysis, hCgB-EYFP fluorescent structures were tracked automatically and displayed as projection to the XY plane (Figure 4B) and three-dimensionally with time as a third (Z) dimension (Figure 4C). The green trajectories depict vesicles moving directed and at high velocities up to 5 µm/s (Figure 4B, arrows). They demonstrate the power and usefulness of this software package for the analysis of fast vesicular dynamics. However, if the trajectories of different vesicles intersect,

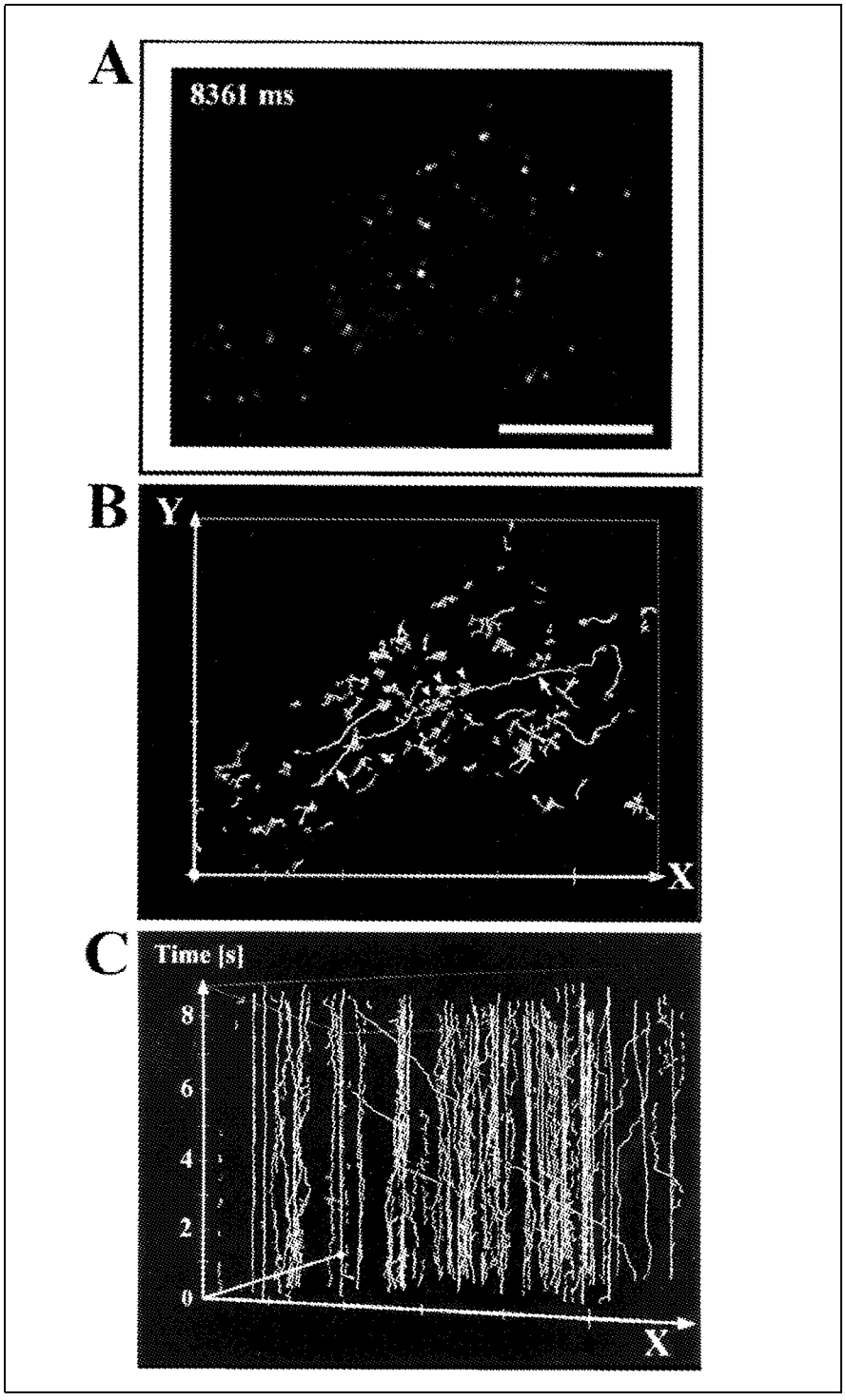

Figure 4. Visualization and automated analysis of fast moving secretory vesicles by high-speed, CCD-based imaging. Vero cells were co-transfected with hCgB-EYFP and phogrin-ECFP and cultivated on LabTek chambers. EYFP was excited using the SP-EYFP filter set (see Materials and Methods) and a 20 ms exposure time. For image acquisition (using a VGA chip-equipped camera), an AOI of 323 × 249 pixels was used. Then, 200 consecutive frames with a cycle time of 42 ms were imaged. The last original frame of this sequence is shown in panel A. The number at the top left indicates the time point of image acquisition and the scale bar at the bottom right represents 10 µm. Trajectories of single vesicles were determined automatically and are displayed in the XY plane (B) and in a three-dimensional view with time evolving along the Z-axis (C). Trajectories indicating fast directed movement over long distances are depicted in green. Red-filled circles in panel B indicate starting points of green trajectories. Arrows in panel B indicate two long trajectories resulting from the automated tracking of one fast moving vesicle crossing the entire cell; arrowheads in panel B indicate intersecting trajectories of other vesicles. A movie of the complete sequence that corresponds to panel A can be viewed at http://www.nbio.uni-heidelberg.de/Gerdes.html.

mistakes in identifying their tracks occurred in some cases. This is exemplified for one long trajectory that traversed the entire cell as verified by manual tracking (not shown). In the automated analysis, this trajectory was split into two pieces (Figure 4B, arrows), most likely due to the intersecting trajectories (arrowheads) combined with a higher local density of identified objects.

The technical feasibility of fast image acquisition rates raises the question whether they are suitable for the analysis of vesicle dynamics and in which cases. First, fast dynamic transport processes may exist that can only be resolved by high image acquisition rates. Notably, by inspection of the described image sequence acquired with 24 frames per second, we have detected a subpopulation of secretory vesicles moving through the entire cell at a speed of approximately 5 μm/s. These vesicles had escaped our attention in previous studies when cells were analyzed with a lower time resolution (16). Velocities in the range of 5 μm/s have so far only been reported for fast axonal transport analyzed by differential interference contrast microscopy (1). Second, the reliability of automated vesicle tracking increases with shorter time distances between subsequent frames. This becomes even more relevant when the density of the observed objects is high. Third, the high image acquisition rates provided by the setup used here open the possibility for at least triple-color imaging of fast dynamic processes (several micrometers per second) with spatial resolution sufficient to resolve small transport vesicles. In this respect, image acquisition in the burst mode would minimize the time shift between the three corresponding channel recordings.

CONCLUSION

Dual-color imaging permits a comparison of the distribution of two different proteins in living cells. This technique has the potential to provide new insights into dynamic interactions of cellular compartments labeled by the respective proteins. For example, the time-dependent recruitment of motor proteins such as kinesins and myosins to transport containers or fusion (Figure 3B) and fission events of distinct membranous structures become accessible. However, an essential requirement for addressing such questions is an accurate determination of colocalization in time and space. Due to the unavoidable time shift caused by sequential image acquisition of the setup used here, colocalization cannot be accurately analyzed by a simple overlay of corresponding channel recordings. To overcome this problem, we calculated colocalization by the interpolated simultaneous position of distinct vesicles in a time-space reconstruction. Even dual-color imaging systems using simultaneous image acquisition will make such sophisticated programs useful because dynamic colocalization is superior in accuracy to a random overlay of still images.

ACKNOWLEDGMENTS

The first three authors contributed equally to this work. We are grateful to Dr. J. Hutton for providing us a plasmid with phogrin cDNA, to M. Maass (Olympus) for his help in initiating this study and to W. Tvaruskó for advice in developing software for analysis of dual color imaging. We also would like to thank W.B. Huttner for continuous support. D.G. was supported by the Graduiertenkolleg "Molekulare und Zelluläre Neurobiologie", R.R. by the Studienstiftung des deutschen Volkes and H.-H.G. was a recipient of a grant from the Deutsche Forschungsgemeinschaft (SFB 317/C7).

REFERENCES

1. **Brady, S.T.** 1991. Molecular motors in the nervous system. Neuron *7*:521-533.
2. **Cubitt, A.B., R. Heim, S.R. Adams, A.E. Boyd, L.A. Gross and R.Y. Tsien.** 1995. Understanding, improving and using green fluorescent proteins. Trends Biochem. Sci. *20*:448-455.
3. **Ellenberg, J., J. Lippincott-Schwartz and J.F. Presley.** 1998. Two-color green fluorescent protein time-lapse imaging. BioTechniques *25*:838-846.
4. **Gerdes, H.-H. and C. Kaether.** 1996. Green fluorescent protein: applications in cell biology. FEBS Lett. *389*:44-47.
5. **Heim, R., A.B. Cubitt and R.Y. Tsien.** 1995. Improved green fluorescence. Nature *373*:663-664.
6. **Heim, R. and R.Y. Tsien.** 1996. Engineering green fluorescent protein for improved brightness, longer wavelengths and fluorescence resonance energy transfer. Curr. Biol. *6*:178-182.
7. **Hermel, J.-M.** 1999. Post-translational modifications of ICA512, a receptor tyrosine phoshatase-like protein of secretory granules. Eur. J. Neurosci. *11*:2609-2620.
8. **Huttner, W.B., H.-H. Gerdes and P. Rosa.** 1991. The granin (chromogranin/secretogranin) family. Trends Biochem. Sci. *16*:27-30.
9. **Kaether, C. and H.-H. Gerdes.** 1995. Visualization of protein transport along the secretory pathway using green fluorescent protein. FEBS Letters *369*:267-271.
10. **Kaether, C., T. Salm, M. Glombik, W. Almers and H.-H. Gerdes.** 1997. Targeting of green fluorescent protein to neuroendocrine secretory granules: a new tool for real time studies of regulated protein secretion. Eur. J. Cell Biol. *74*:133-142.
11. **Lippincott-Schwartz, J. and C.L. Smith.** 1997. Insights into secretory and endocytic membrane traffic using green fluorescent protein chimeras. Curr. Opin. Neurobiol. *7*:631-639.
12. **Matlin, K.S. and K. Simons.** 1983. Reduced temperature prevents transfer of a membrane glycoprotein to the cell surface but does not prevent terminal glycosylation. Cell *34*:233-243.
13. **Pouli, A.E., E. Emmanouilidou, C. Zhao, C. Wasmeier, J.C. Hutton and G.A. Rutter.** 1998. Secretory-granule dynamics visualized in vivo with a phogrin-green fluorescent protein chimaera. Biochem. J. *333*:193-199.
14. **Tsien, R.Y.** 1998. The green fluorescent protein. Annu. Rev. Biochem. *67*:509-544.
15. **Tvaruskó, W., M. Bentele, T. Misteli, R. Rudolf, C. Kaether, D.L. Spector, H.-H. Gerdes and R. Eils.** 1999. Time-resolved analysis and visualization of dynamic processes in living cells. Proc. Natl. Acad. Sci. USA *96*:7950-7955.
16. **Wacker, I., C. Kaether, A. Krömer, A. Migala, W. Almers and H.-H. Gerdes.** 1997. Microtubule-dependent transport of secretory vesicles visualized in real time with a GFP-tagged secretory protein. J. Cell Sci. *110*:1453-1463.
17. **Wasmeier, C. and J.C. Hutton.** 1996. Molecular cloning of phogrin, a protein-tyrosine phosphatase homologue localized to insulin secretory granule membranes. J. Biol. Chem. *271*:18161-18170.
18. **Zimmermann, T. and F. Siegert.** 1998. Simultaneous detection of two GFP spectral mutants during in vivo confocal microscopy of migrating *Dictoystelium* cells. BioTechniques *24*:458-461.

Received 28 September 1999; accepted 1 December 1999.

Address correspondence to:

Dr. Hans-Hermann Gerdes
Dept. of Neurobiology
University of Heidelberg
Im Neuenheimer Feld 364
69120 Heidelberg, Germany
Internet: hhgerdes@sun0.urz.uni-heidelberg.de